Chemistry–A European Journal
Research Article
doi.org/10.1002/chem.202301073
Chemistry Europe
European Chemical Societies Publishing
www.chemeurj.org

From Terminal to Spiro-Phosphonium Acceptors, Remarkable Moieties to Develop Polyaromatic NIR Dyes

Iida Partanen,[a] Andrey Belyaev,*[a, b, c] Bo-Kang Su,[d] Zong-Ying Liu,[d] Jarkko J. Saarinen,[a] Ishfaq Ibni Hashim,[a] Andreas Steffen,[b] Pi-Tai Chou,*[d] Carlos Romero-Nieto,*[e, f] and Igor O. Koshevoy*[a]

Abstract: Phosphonium-based compounds gain attention as promising photofunctional materials. As a contribution to the emerging field, we present a series of donor-acceptor ionic dyes, which were constructed by tailoring phosphonium (A) and extended π-NR_2 (D) fragments to an anthracene framework. The alteration of the π-spacer of electron-donating substituents in species with terminal $-^{+}PPh_2Me$ groups exhibits a long absorption wavelength up to $\lambda_{abs} = 527$ nm in dichloromethane and shifted the emission to the near-infrared (NIR) region ($\lambda = 805$ nm for thienyl aniline donor), although at low quantum yield ($\Phi < 0.01$). In turn, the introduction of a P-heterocyclic acceptor substantially narrowed the optical bandgap and improved the efficiency of fluorescence. In particular, the phospha-spiro moiety allowed to attain NIR emission (797 nm in dichloromethane) with fluorescence efficiency as high as $\Phi = 0.12$. The electron-accepting property of the phospha-spiro constituent outperformed that of the monocyclic and terminal phosphonium counterparts, illustrating a promising direction in the design of novel charge-transfer chromophores.

Introduction

Decoration of polyaromatic hydrocarbons (PAHs) with main group heteroelements such as boron, nitrogen, oxygen, sulfur and phosphorus has been recognized as an efficient strategy to expand the reactivity and to remarkably modify the electronic properties of the conjugated systems.[1] Gaining control over the energies of frontier molecular orbitals and tuning the S_1–S_0 energy gap play a pivotal role in the rational molecular design for organic compounds with desired photophysical characteristics for optoelectronic, sensing and bioimaging applications.[2]

Photofunctional organophosphorus derivatives of PAHs primarily comprise stable chalcogenated ($\lambda^5\sigma^4$) and quaternized cationic ($\lambda^4\sigma^4$) P-centers,[3] which can be tailored to the parent hydrocarbon core as (i) pendant substituent(s) or (ii) merged with it to produce extended heterocyclic motifs. Thus, the mono- and disubstituted anthracenes bearing $-PPh_2E$ units (E=O, S, Se) demonstrated intriguing solid-state photophysical properties due to non-covalent intermolecular interactions and excimer formation, which in turn depend on the chemical nature of the phosphino-chalcogenide and its position on the PAH fragment.[4] The electron-accepting nature of the phosphine oxide groups allowed some of these and analogous compounds to be employed as emitting and host materials in electroluminescent devices.[5] In addition, due to the versatile connectivity of the phosphorus atom, several polyaromatic motifs can be combined at the same phosphorus center in $(PAH)_nR_{3-n}P{=}E$ (n = 1–3) molecules.[6] Despite a relative facileness

[a] I. Partanen, Dr. A. Belyaev, Prof. J. J. Saarinen, I. Ibni Hashim, Prof. I. O. Koshevoy
Department of Chemistry
University of Eastern Finland
Yliopistokatu 7, 80101 Joensuu (Finland)
E-mail: igor.koshevoy@uef.fi
andrei.a.beliaev@jyu.fi

[b] Dr. A. Belyaev, Prof. A. Steffen
Faculty of Chemistry and Chemical Biology
TU Dortmund University
44227 Dortmund (Germany)

[c] Dr. A. Belyaev
Department of Chemistry/Nanoscience Center
University of Jyväskylä
Survontie 9 C, 40014 Jyväskylä (Finland)

[d] B.-K. Su, Z.-Y. Liu, Prof. P.-T. Chou
Department of Chemistry
National Taiwan University
Taipei, Taiwan 10617 (ROC)
E-mail: chop@ntu.edu.tw

[e] Prof. C. Romero-Nieto
Institute of Organic Chemistry
Heidelberg University
Im Neuenheimer Feld 270 D-69120 Heidelberg (Germany)
E-mail: carlos.romero.nieto@oci.uni-heidelberg.de

[f] Prof. C. Romero-Nieto
Faculty of Pharmacy
Universidad de Castilla-La Mancha
Calle Almansa 14 - Edif. Bioincubadora, 02008, Albacete, (Spain)

Supporting information for this article is available on the WWW under https://doi.org/10.1002/chem.202301073

of synthesis process, polyaromatic chromophores with terminally appended $\lambda^5\sigma^4$ or $\lambda^4\sigma^4$ phosphorus groups and the reports on their photophysical behavior are not excessive, probably because of limited tunability of the electron-withdrawing characteristics of these pendant constituents.

Owing to the flourishing photoelectronic material research in these years, the applications of P-heterocyclic photofunctional PAHs have demonstrated a more extensive growth. A selection of five-,[7] six-,[8] and higher-membered[9] phosphacycles has been successfully integrated into polyaromatic scaffolds offering spectacular modulation of electronic and optical properties. The latter has been achieved following three main directions – (i) the variation of the PAH and heterocyclic motifs,[7b,d,f,g,10] (ii) the variation of the acceptor strength of the phosphorus center,[7b,8b,10a,11] (iii) induction of intramolecular charge transfer (ICT) in donor-acceptor molecules.[12] As a result, a diversity of phosphorus-containing polyaromatic compounds, which predominantly comprise the phosphole moiety, have been designed to exhibit appealing responsive,[13] self-assembling,[14] switchable,[14a,15] and electron-transporting[16] behavior. Furthermore, the good stability of selected species meets the requirements of light-emitting diodes,[7d,f] photovoltaics,[17] semiconducting materials[11a] and super resolution spectroscopy.[12a,18]

Despite impressive progress in the field, donor-acceptor (D–A) architectures in organophosphorus polyaromatic chromophores have only been utilized to a limited extent.[12a,18–19] However, D–A motifs offer efficient means to narrow the S_1–S_0 energy gap of the conjugated systems. This is important because it allows shifting the absorption and emission to the low-energy region, even reaching elusive near-infrared (NIR) optical properties and improving the light-harvesting and two-photon absorption capacities. In fact, numerous investigations have been carried out in recent years to develop suitable NIR-emitting organophosphorus chromophores for bio-imaging due to their outstanding performance as bio-markers.[18,20]

In our previous work, we reported a series of D–A systems composed of naphthalene, phenanthrene and anthracene building blocks and heterocyclic phosphonium dyes.[21] By tailoring the electron-donating $-NR_2$ groups and using the distinct electron-accepting properties of quaternized $-^+PR_2-$ phosphacycles, we succeeded in achieving the record at that time for the dye with the most shifted emission maxima in near infrared, based on phosphorus heterocycles.[21] It showed high fluorescence quantum yield of 0.18 in CH_2Cl_2 and an emission maximum at 780 nm. However, recent studies[22] on the modulation of the accepting properties of phosphorus by hyperconjugative effects pointed out the spiro-like quaternized phosphorus atoms to be the strongest electron-accepting groups based on phosphorus centers and not the $-^+PR_2-$. Nevertheless, even though the first phospha-spiro compound was reported in 1966 by Hellwinkel,[23] experimentally, the spectroscopic properties of these bicyclic species are still virtually unknown.

In views of such precedents, we performed the first comprehensive investigation on the phosphonium-based D–A dyes including the phospha-spiro derivatives.

Our results show that indeed the bicyclic acceptor fragment leads to breaking the record of NIR emitting organophosphorus chromophores. Among all the species in this study, the one with phospha-spiro architecture shows an emission maximum at 797 nm with appreciable fluorescence quantum yield in solution, further shifted to 860 nm in the solid state. Thus, our investigations establish the phospha-spiro-based dyes as a new class of compounds with promising potential for luminescent (bio)applications.

Results and Discussion

Synthesis and Characterization

The investigated dyes comprise a phosphonium center at the anthracene chromophore core (Figure 1). Compounds **1**–**3**[X] feature a 6-membered P-heterocycle fused with a polyaromatic motif (X = anion). Triflate salts **1**[OTf] and **2**[OTf] were reported by us earlier.[21] To check the effect of bulky counterion and minimize cation-cation interactions in the solid state, **1**[OTf] and **2**[OTf] were converted into derivatives **1**[BAr^F_4] and **2**[BAr^F_4] with tetrakis[3,5-bis(trifluoromethyl)phenyl]borate ($^-BAr^F_4$) by metathesis reaction (see the Supporting Information for experimental details). Whereas **1**[BAr^F_4] and **2**[BAr^F_4] differ by the donor-containing fragment, we intended to amend the characteristics of the electron-deficient phosphacyclic part.

For this purpose, the dibenzophosphole fragment, which has a pronounced electron-accepting behavior thanks to the hyperconjugative effects,[3a] was conjoined with the parent anthracene-P-heterocyclic core (**3a**[OTf] and **3**[OTf]). The synthesis of the new P-spiro compounds **3a**[OTf] and **3**[OTf] is outlined in Scheme 1. In brief, the $\lambda^3\sigma^3$-phosphole precursors **p1**

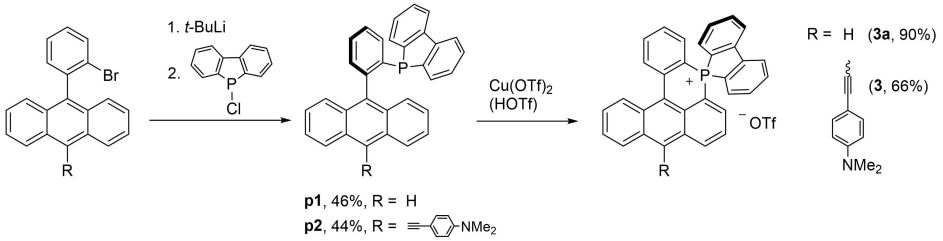

Scheme 1. Synthesis of compounds **3a**[OTf] and **3**[OTf].

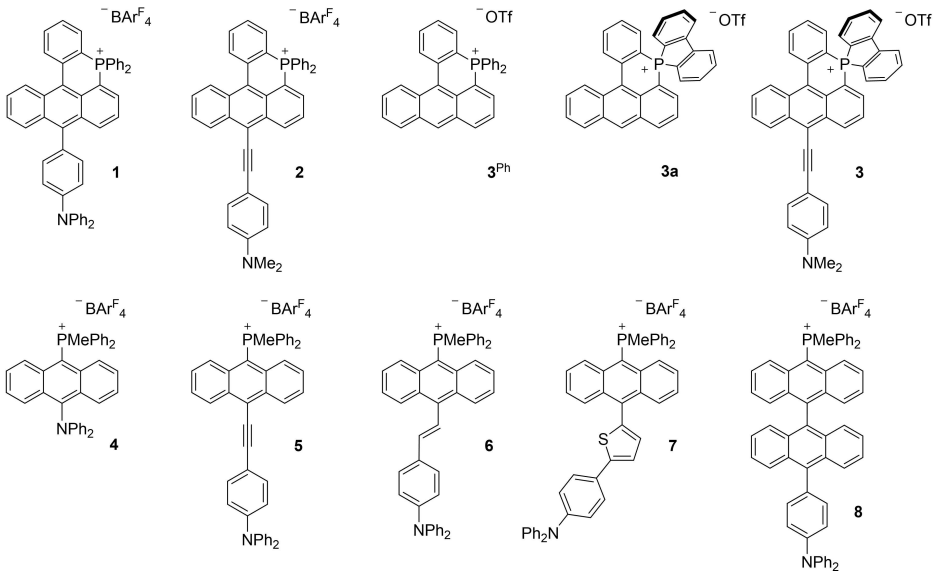

Figure 1. Anthracene-based phosphonium salts considered in this work (compound **3**^{Ph}[OTf][21] with cyclized P atom bearing phenyl substituents is included for comparison with bicyclic **3a**[OTf]).

and **p2** were obtained in moderate yields (44–46%) from the lithium-halogen exchange of the 9-(2-bromophenyl)anthracene[21] with *t*-BuLi followed by the reaction with 5-chloro-dibenzo[*b,d*]phosphole.[24] Quaternization of the phosphorus center, which leads to the 6-membered phosphacycle, proceeds upon treatment of phospholes **p1** and **p2** with 2 equivalents of copper(II) triflate according to the developed protocol.[21,25] While the cyclization of **p1** to give **3a**[OTf] is efficiently mediated by $Cu(OTf)_2$ in acetonitrile-dichloromethane solution at room temperature, the reaction from the donor-functionalized **p2** under the same conditions produces salt **3**[OTf] in low yields of ca. 10% and required tedious purification. However, the addition of triflic acid (2 equivalents, ambient conditions) together with $Cu(OTf)_2$ apparently protonates the starting aniline-containing phosphole **p2** and dramatically improves the yield of **3**[OTf] to 66%.

The second group of D–A dyes (**4**–**8**[BAr$^F_4$]) are the 9,10-substituted anthracenes having terminal $-^+PPh_2Me$ phosphonium group as an acceptor A and variable donor fragment D (Figure 1). These cations are obtained in moderate yields by straightforward methylation of tertiary phosphines (Scheme 2), analogously to the earlier synthesis of the iodide salt **4**[I].[26] Subsequent metathesis of the iodide for the $^-BAr^F_4$ anion was carried out due to limited stability of the initial D–A phosphonium iodides and significant emission quenching in the presence of I^-.

The identity of cations **1**–**8**[X] was confirmed by ESI$^+$ mass spectra, which showed the dominating signals at $m/z = 680.25$, 580.22, 578.20, 544.22, 644.25, 646.26, 702.23, 796.30 corresponding to singly charged molecular ions, respectively (Supporting Information). Each of the title compounds displays a singlet peak in the $^{31}P\{^1H\}$ NMR spectrum from CD_2Cl_2 solutions, which is found in the range 5.7–6.7 ppm for phosphacyclic species **1**–**3**[X], and 17.8–18.3 ppm for terminally phosphonium-decorated anthracenes **4**–**8**[BAr$^F_4$]. A minor downfield shift of ca. 1 ppm of the signals from the spiro compounds **3a** and **3** compared to **1** and **2** likely originates from somewhat lower electron density and thus deshielded phosphorus nucleus in the phosphole-containing cations. The values of chemical shifts are compatible with the data obtained for other structurally related species[10d,21,26–27] and are virtually independent of the nature of anions indicating a lack of ion pair association in polar solvents.

The structures of dyes **2**[BAr$^F_4$] and **3a**[OTf] were determined crystallographically and are depicted in Figure 2 (Tables S1 and S2 list the crystal data and selected bond lengths and angles, respectively). Cation **3a**$^+$ is a rare example of spirocyclic systems with $\lambda^4\sigma^4$ P-center, which so far have been

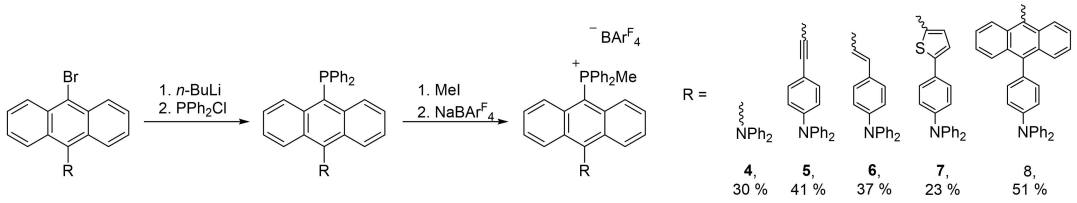

Scheme 2. Synthesis of compounds **4**–**8**.

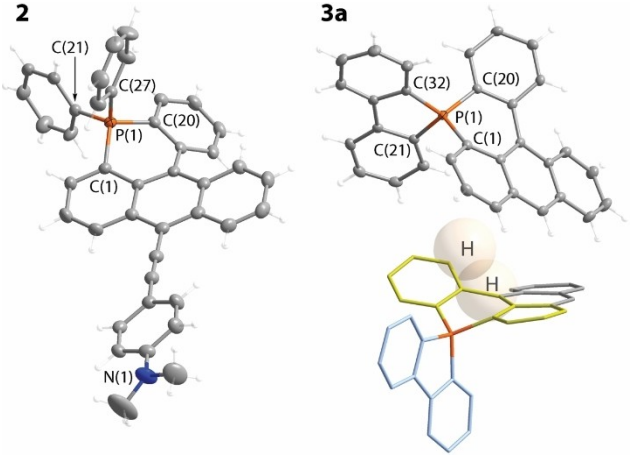

Figure 2. Molecular views of phosphonium salts **2**[BAr^F_4] (left) and **3a**[OTf] (right, the bottom view highlights geometrical distortions due to repulsion of hydrogen atoms shown in a space-filling mode). Thermal ellipsoids are given at the 50% probability level. Counterions are omitted for clarity.

mainly represented by symmetrical spirobiphosphoniafluorenes.[28] Both cations in $\mathbf{2}^+$ and $\mathbf{3a}^+$ demonstrate substantial deviation of the PAH-heterocyclic framework from planarity, which is evidently caused by steric hindrance between the hydrogen atoms of the phenylene and anthracene fragments. As a result, the tetrahedral phosphorus atoms in $\mathbf{2}^+$ and $\mathbf{3a}^+$ clearly lie out of the average plane of the polyaromatic core, which in turn demonstrates a certain curvature distortion.[21] Contrarily to the six-membered ring, the phosphole motif in $\mathbf{3a}^+$ adopts a typical planar configuration and is nearly orthogonal with respect to the anthracene part.

Salt **2**[BAr^F_4] reveals some intermolecular π-π stacking interactions between the alkynyl-PAH chromophores of adjacent cations, which demonstrate "head-to-tail" orientation, and relatively long (>3.8 Å) cation-BAr^F_4 anion π-contacts (Figure S1). Most likely, such interaction significantly perturbs the main skeleton's linearity and leads to a tilted and twisted conformation of the D and anthracene cores of $\mathbf{2}^+$. No appreciable stacking is observed in the crystal packing of compound **3a**[OTf].

Spectroscopic Properties and Theoretical Analysis

To get the first insights into the photophysical properties of molecules **1**–**8** (Figure 1), we carried out DFT calculations at the B3LYP/6-311+G(d) level with CH_2Cl_2 as solvent under the PCM solvent model (Figures S2–S6, and Table S3). The optimized structures of the cations are consistent with the crystallographic data, including the nonplanarity of the phospha-cyclic compounds. Assuming that in polar solvent the effect of ion pairing is negligible, the counteranions were not included into the models. For all cations, the LUMO is largely distributed at the electron-deficient phosphonium fragment, while the HOMO, except for **3a**, is located at the electron-donating amino fragment. It is important to note that the LUMO of the spiro-derivatives **3a** and **3** is also delocalized over the fluorene fragment (Figure 3), which was attributed to a phenomenon of 3D conjugation occurring in a non-planar bicyclic system between the six-membered phosphorus heterocycle and the bisphenyl fragment.[22] **8** significantly differs structurally from the rest of the derivatives since it presents a perpendicularly arranged bianthracene core. Regarding the relative energy of the molecular orbitals, compound **3**, a D–A system with a phospha-spiro moiety, shows the narrowest S_1–S_0 energy gap of 2.14 eV. Comparison of the results with those of compound **2**, the analogous derivative with a $-^+PR_2-$ fragment and a S_1–S_0 energy difference of 2.18 eV, reveals that the spiro motif is indeed a stronger electron-accepting group, which further reduces the S_1–S_0 energy gap of the D–A chromophore. This can also be evidenced by a decrease in LUMO energy from −3.28 to −3.32 eV for **2** and **3**, respectively, while the HOMO remains practically unchanged, i.e. −5.46 and −5.47 eV for **2** and **3**. The electrochemical study of **3** shows an irreversible oxidation at +0.95 V and multiple reduction processes. The first accessible reduction waves are at −0.75, −1.18 and −1.50 V (Figure S7), which are more positive than for **2**[OTf] (−0.79, −1.25 and −1.95 V)[21] indicating better electron-accepting properties of the spiro motif. In turn, the importance of the D–A architecture for decreasing the S_1–S_0 energy gap is apparent

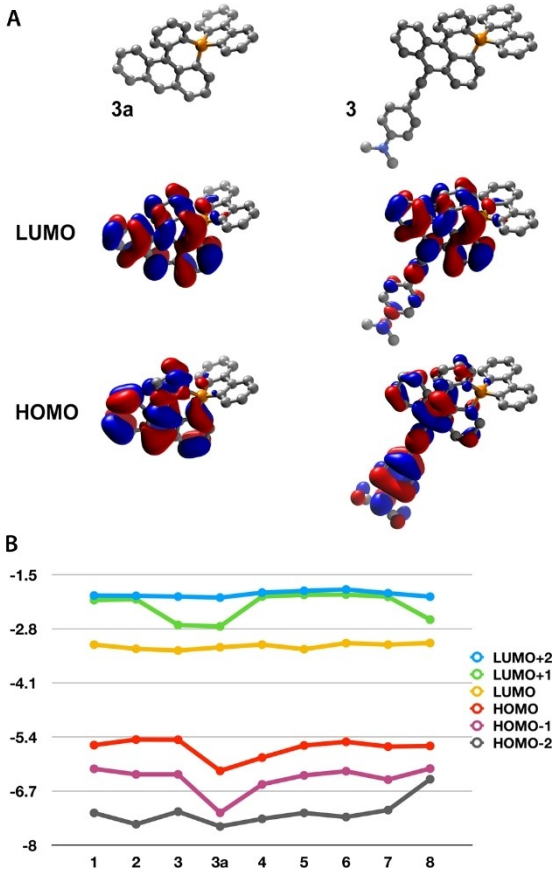

Figure 3. A: frontier molecular orbitals of phospha-spiro derivatives **3a** and **3** obtained by DFT calculations. B: representation of the energies of the molecular orbitals (eV) for compounds **1** to **8** computed by DFT calculations.

when comparing the properties of **3** with those of **3 a** that lacks the extended *para*-ethynylphenyldimethyl amino donor group. While the LUMO level is only relatively increased from −3.32 to −3.24 eV from **3** to **3 a**, the HOMO starkly decreases from −5.47 to −6.22 eV for **3** to **3 a** as a result of a lower electronic density in the system. The latter results in a strong increase in the S_1–S_0 energy gap from 2.14 eV for **3** to 2.97 eV for **3 a**, which is the largest value for the entire series **1**–**8** (Table S3). Theoretical attempts to find better donating π-extended fragments for further reducing the S_1–S_0 energy gap were unsuccessful. Changing the nature of the donating moiety on anthracene derivatives containing a quaternized phosphorus atom revealed the *para*-ethynylphenyl amino moiety to be the most electron-donating fragment. Reducing the conjugation by removing the *para*-ethynylphenyl fragment, replacing the triple bond with a double bond, or modifying the nature of the π-spacer by a thiophene or anthracene only led to bigger predicted S_1–S_0 energy gaps. In particular, the S_1–S_0 energy gap is 2.72 eV for **4** and 2.31 eV for **5**. Unexpectedly, replacing the triple bond with a double bond resulted in a S_1–S_0 energy gap of 2.37 eV (**6**). The given difference correlates with the electronic absorption spectra for **5** and **6** (Table 1, Figure 5). This somewhat unexpected behavior contrasts with that of structurally similar donor-acceptor pyridinium[29] and sulfanyl dyes,[30] in which the ones with vinylene spacer exhibit lower energy absorption compared to the ethynyl congeners. Compound **7** with a thiophene spacer instead of a double bound displays a S_1–S_0 energy gap of 2.45 eV, which is increased to 2.48 eV for **8** due to breaking the conjugation within the twisted bianthracene fragment (see Figure S3).

The results from the theoretical investigations were corroborated experimentally by steady-state and time-resolved spectroscopy. Photophysical properties of dyes **1**–**8**[X] in solution are listed in Table 1. In dichloromethane, phosphacyclic compounds **1**–**3** feature low energy (LoE) absorption bands maximized at 484 (**1**[BAr^F_4]), 570 (**2**[BAr^F_4]) and 575 nm (**3**[OTf]) (Figure 4), which are consistent with the ICT nature predicted by theoretical calculations. The absorption wavelengths for salts **1**[BAr^F_4] and **2**[BAr^F_4] are very similar to those for their triflate analogs,[21] which reveals a limited effect of ion pairing in the ground state and negligible charge transfer between anion and cation. The bathochromic shift of the absorption maxima of the spiro-compound **3**[OTf] with respect to **2**[X], both of which comprise the same electron-donating group, confirms the better electron-accepting properties of the phospha-spiro moiety compared to the monocyclic phosphonium fragment in **2**[X], resulting in a smaller energy gap. This trend is observed for **3 a**[OTf] and its mono P-cyclic congener **3**^{Ph}[OTf] (Figure 1),[21] for which the LoE absorption in water is somewhat blue-shifted for approx. 309 cm^{-1} (Figure S8).[21]

The acyclic dyes **4**–**7**[BAr^F_4] show charge transfer bands in the range 497–527 nm (in CH_2Cl_2, Figure 5, and in toluene, Figure S9) in accordance with their D–A molecular structure. These data indicate that embedding the phosphonium and

Table 1. Photophysical properties of **1**–**8**[X] in solution at 298 K.

dye	solvent	λ_{abs}, nm [ε, 10^{-3} M^{-1} cm^{-1}]	λ_{em}, nm	Δν, cm^{-1}	Φ_{em}[a]	τ, ns
1[BAr^F_4]	CH_2Cl_2	277 (42), 484 (8.5)	755	7416	0.05	3.6[b]
	toluene	479 (7.8)	718	6949	0.25	
2[BAr^F_4]	CH_2Cl_2	277 (28.3), 568 (16.6)	776	4719	0.07	1.3[c]
	toluene	578 (15.6)	759	4126	0.12	
2[OTf][21]	CH_2Cl_2	276 (27.6), 570 (17.4)	778	4723	0.18	1.5
3 a[OTf]	CH_2Cl_2	274 (32.0), 458 (7.2)	540	3316	0.99	13.8
	water	271 (40.9), 444 (7.1)	550	4341	0.79	14.6
3^{Ph}[OTf][21]	water	272 (37.6), 438 (6.7)	533	4070	0.99	16.0
3[OTf]	CH_2Cl_2	286 (22.2), 575 (15.3)	797	4844	0.12	1.0
3[BAr^F_4]	toluene	586	780	4244	0.09	1.1
4[BAr^F_4]	CH_2Cl_2	265 (86.7), 520 (6.5)	720	5342	0.03	2.8[b]
	toluene	526 (6.0)	700	4726	0.02	
5[BAr^F_4]	CH_2Cl_2	266 (28.6), 527 (12.9)	780	6155	0.03	0.7[c]
	toluene	541 (11.9)	704	4280	0.16	
6[BAr^F_4]	CH_2Cl_2	269 (35.9), 497 (6.3)	796	7558	< 0.01	0.4[c]
	toluene	516 (7.6)	710	5295	< 0.01	
7[BAr^F_4]	CH_2Cl_2	357 (42), 502 (9)	805	7498	< 0.01	
	toluene	360 (44), 515 (11)	708	5293	< 0.01	
8[BAr^F_4]	CH_2Cl_2	414	513/790	4661/11496	< 0.01	0.7[c]
	toluene	415	474/700	3057/9869	< 0.01	
	EA	413	503	4333	< 0.01	
	THF	413	477	3250	< 0.01	

[a] The experimental error is ±5 %. [b] Monitored at 680 nm. [c] Monitored at 800 nm.

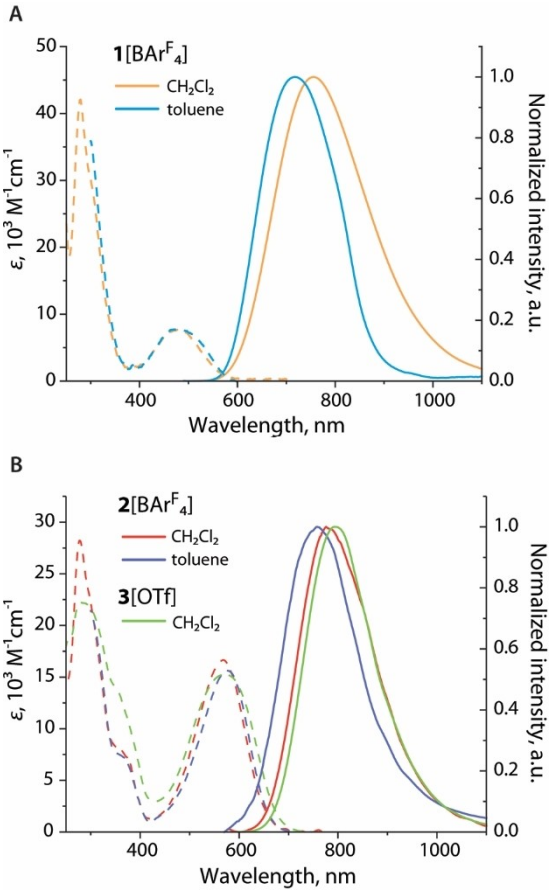

Figure 4. UV-vis absorption (dashed) and emission (solid) spectra of the **1**[BAr^F_4] (A), **2**[BAr^F_4] and **3**[OTf] (B) in CH_2Cl_2 and toluene at 298 K.

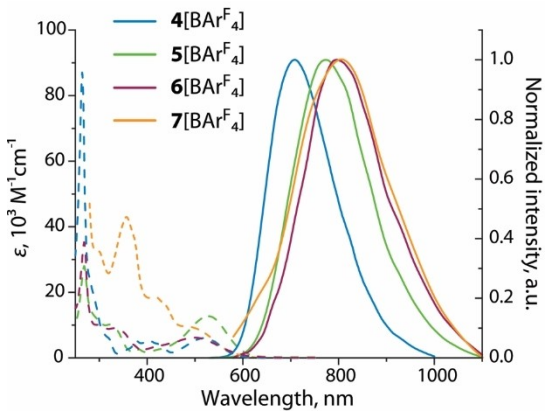

Figure 5. UV-vis absorption (dashed) and normalized emission (solid) spectra of **4**–**7**[BAr^F_4] in CH_2Cl_2 at room temperature.

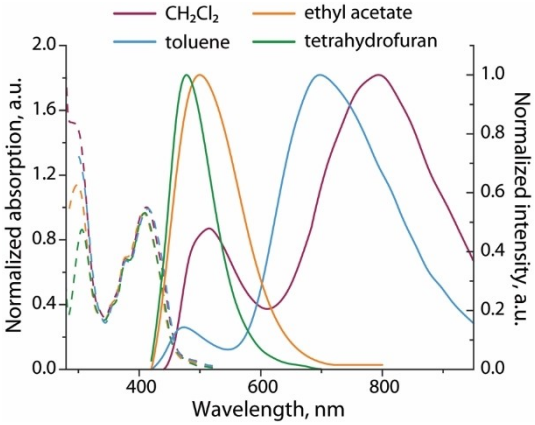

Figure 6. Normalized UV-vis absorption (dashed) and emission (solid) spectra of **8**[BAr^F_4] in toluene, CH_2Cl_2, ethyl acetate and tetrahydrofuran.

disruption of the conjugation between the donor and acceptor functions due to twisted arrangement of two anthracene motifs.

The high solubility of the salts containing $^-BAr^F_4$ anion in toluene allowed for measuring the properties of **1**–**8**[BAr^F_4] in a medium of lower polarity. All compounds with ICT except **8**[BAr^F_4] showed small negative solvatochromism; i.e. an increase of the LoE absorption wavelengths with the decrease of the solvent polarity (Table 1, Figure 4).

This behavior is typical for ionic dipolar chromophores and reflects destabilization/stabilization of the ground/excited state by less polar solvent molecules via dipole-dipole interactions.[31] The absorption wavelength of salt **8**[BAr^F_4] is little affected by the change of the solvent (toluene, CH_2Cl_2, ethyl acetate, tetrahydrofuran), which further supports a reduced intramolecular photoinduced charge transfer (Table 1, Figure 6).

In line with the absorption properties, the emission spectra of **1**[BAr^F_4] and **2**[BAr^F_4] in CH_2Cl_2 (λ_{em}/Φ_{em} = 755 nm/0.05 and 776 nm/0.07, Figure 4) resemble those of the corresponding triflates (λ_{em}/Φ_{em} = 760 nm/0.1 and 778 nm/0.18).[21] Albeit in solution counterions have a minor influence in the emission wavelengths, quantum yields for $^-BAr^F_4$ salts are at least twice lower than those for the $^-$OTf analogs due to a decrease of the radiative rate constants ($k_r = 1.3\times10^7$ and $5.4\times10^7\ s^{-1}$ for **1**[BAr^F_4] and **2**[BAr^F_4] vs 2.9×10^7 and $1.2\times10^8\ s^{-1}$ for triflates), while the nonradiative rates are affected to a much smaller extent. This discrepancy indicates that the given bulky counterion somehow affects the transition dipole moment by different degrees of the ion-pair interaction, and hence changes the radiative decay rate constant. It is worth mentioning the behavior of **2**[BAr^F_4] in toluene, where the long wavelength tail extends beyond 1100 nm and clearly surpasses that of the emission profile in CH_2Cl_2. This feature may arise from ion migration phenomenon, which occurs in non-dissociated ion pairs of D–A dyes in non-polar solvents and generates the low energy emission bands.[26,32]

The phospha-spiro derivative **3a** exhibits an emission maximum at 540 nm in CH_2Cl_2 with an impressively high

especially the phospha-spiro motifs into the polycyclic system is more beneficial for attaining the redshifted absorption than the terminal decoration. In contrast to the abovementioned species, the biacene compound **8**[BAr^F_4] exhibits the most hypsochromically shifted absorption maximum (414 nm in CH_2Cl_2, Figure 6), which, in accordance with theoretical calculations, supports the

fluorescence quantum yield of 0.99, while the D–A compound **3** with a spiro fragment exhibits the longest emission wavelength known to date from phosphorus heterocycles at 797 mn and still maintaining a remarkable emission quantum yield of 0.12 (Figures 4 and S8). The fluorescence bands of compounds **3a** and **3** are bathochromically shifted for ca. 749 and 273 cm^{-1} (ca. 20 nm) compared to the previously reported non-spiro phosphonium relatives, λ_{em}/Φ_{em} = 519 nm/0.69 and 780 nm/0.18 in CH_2Cl_2, respectively.[21] This reaffirms the important role of the phospha-spiro fragments vs other quaternized phosphorus centers in tuning the optical properties of D–A systems, particularly in achieving the NIR emission. Note that NIR photoluminescence is highly desirable for bioimaging applications and some organophosphorus dyes have been demonstrated to be especially suited to that end.[18,20,33] Finally, salt **3a**[OTf] retains intense yellow-greenish fluorescence in water (λ_{em} = 550 nm, Figure S8) with the quantum yield of 0.79.

The luminescence characteristics of compounds **4**–**7**[BAr^F_4] with terminal $-^+PPh_2Me$ phosphonium group strongly depend on the nature of the spacer between the $-NPh_2$ moiety and the anthracene core (Scheme 2). The emission energy in dichloromethane gradually decreases in the order of **4** (λ_{em} = 720 nm) > **5** (λ_{em} = 780 nm) > **6** (λ_{em} = 796 nm) > **7** (λ_{em} = 805 nm), (Figure 5). Importantly, this trend does not show any correlation with that of the absorption maxima, indicating a complex dynamic process upon photoexcitation. Even though the emission wavelength of **7** is slightly longer than that of **3**, it is worth noting that **7** exhibits a fluorescence quantum yield < 0.01. The fluorescence of **4**[BAr^F_4] in dichloromethane is very similar to that of the previously reported iodide **4**[I] (λ_{em}/Φ_{em} = 720 nm/0.02),[26] which implies little influence of the anions on the photophysics of chromophoric cations in polar solvents like CH_2Cl_2 .[34] The emission bands of **3**[BAr^F_4] and **6**[BAr^F_4] maximize virtually at the same wavelengths in CH_2Cl_2, but the quantum yield for **6**[BAr^F_4] (Φ_{em} < 0.01) is ca. two orders of magnitude lower than that for **3**[BAr^F_4]. This highlights the benefits of the rigid phospha-spiro structure on the suppression of non-radiative relaxation pathway.

In toluene, salts **1**–**7**[BAr^F_4] manifest hypsochromic shift of luminescence ranging from 273 cm^{-1} (Δ17 nm, **2**) to 1702 cm^{-1} (Δ97 nm, **7**), Figures 4 and S9. This positive solvatochromism is accompanied by a decrease in Stokes shift, which is primarily caused by the increase in the emission energy and suggests smaller structural change occurring in the excited state. The latter can be tentatively attributed to the formation of ion pairs, in which the $^-BAr^F_4$ counterion, the size of which is comparable to that of the cationic chromophore, destabilizes the ICT S_1 state due to photoinduced charge redistribution and the lack of bulky anion relocation occurring for smaller anions.[26,32] Most of the dyes (**1**, **2**, **4**–**7**)[BAr^F_4] in toluene exhibit higher quantum yields than in dichloromethane with up to a 5-fold increase for **1** and **5** (Table 1).

This enhancement is presumably caused by the aforementioned increase in the emission energy, although the rigidifying effect of the large anion cannot be ruled out for non-dissociated ion pair.

The diacene compound **8**[BAr^F_4], which is one of the weakest emitters in the studied series, unveils a more complicated solvent-dependent fluorescence (Figure 6). While in tetrahydrofurane and ethyl acetate the spectra comprise one high energy (HiE) band (477 and 503 nm, respectively), in dichloromethane and toluene **8**[BAr^F_4] is dually emissive with dominating LoE signal at 790 and 700 nm, respectively. The excitation spectra monitored at two emission wavelengths (Figure S10) confirm that both bands originate from the same excited species. The HiE band is plausibly assigned to the locally excited (anthracene) state, which corresponds to the orthogonal conformation of the biacene core, as it has been described for other bianthryl molecules.[35] The appearance of the NIR band patently arises from torsional relaxation that favors the formation of the LoE twisted charge transfer (TICT) state.

In the solid state, the luminescence of ionic dyes often depends on the nature of counterions, which affect the packing and intermolecular interactions.[34b,36] As a matter of fact, sterically demanding fluorinated aryl borates have been used to minimize the detrimental aggregation-induced quenching by isolating the chromophore centers in polymer matrix, and in some cases caused a red-shifted emission.[37] The solid-state fluorescence of **1**–**8**[BAr^F_4] and **3**[OTf] was studied from neat amorphous samples (Table 2). Dual emission with the maxima at 650 and 850 nm and a total quantum yield of 0.02 was detected for compound **1**[BAr^F_4] (Figure 7). Grinding the sample did not change substantially the ratio and the position of the bands. Two different excited states could emerge from distinct molecular conformations with variable degrees of charge transfer rather than from intermolecular aggregates since the latter are typically sensitive to mechanical perturbation. The emission of **2**[BAr^F_4] (λ_{em} = 696 nm) was considerably blue-shifted (ca. 1481 cm^{-1} or 81 nm) relative to that in CH_2Cl_2 solution, while for **2**[OTf] it was strongly red-shifted to the NIR region ca. 2246 cm^{-1} (129 nm) to λ_{em} = 825 nm. The spiro derivative **3**[OTf] also showed the lowest energy fluorescence maximum at 860 nm in the solid state. In a similar fashion to **2**[X], the exchange of the counterion in **3** from OTf^- to bulky $^-BAr^F_4$ produces a significant hypsochromic shift of the emission (1030 cm^{-1}, Figure 7A). The highest NIR luminescence quantum yield of the title solid dyes was found for the terminal phosphonium salt **6**[BAr^F_4] with a styryl spacer (λ_{em}/Φ_{em} =

Table 2. Photophysical properties of **1**–**8**[X] in the solid state at room temperature.

Dye	λ_{em}, nm	Φ_{em}	τ, ns
1[BAr^F_4]	650/830	0.02	1.5[a]
2[BAr^F_4]	696	0.02	7.0[b]
2[OTf]	825	n.d.	n.d.
3a[OTf]	575	0.35	0.8 (0.74), 3.3 (0.26)
3[OTf]	860	n.d.	n.d.
3[BAr^F_4]	790	n.d.	n.d.
4[BAr^F_4]	666	0.04	6.8[b]
5[BAr^F_4]	695	< 0.01	3.7[b]
6[BAr^F_4]	740	0.04	0.9[b]
7[BAr^F_4]	670	< 0.01	n.d.
8[BAr^F_4]	630	0.01	6.9[a]

[a] Monitored at 650 nm. [b] Monitored at 700 nm.

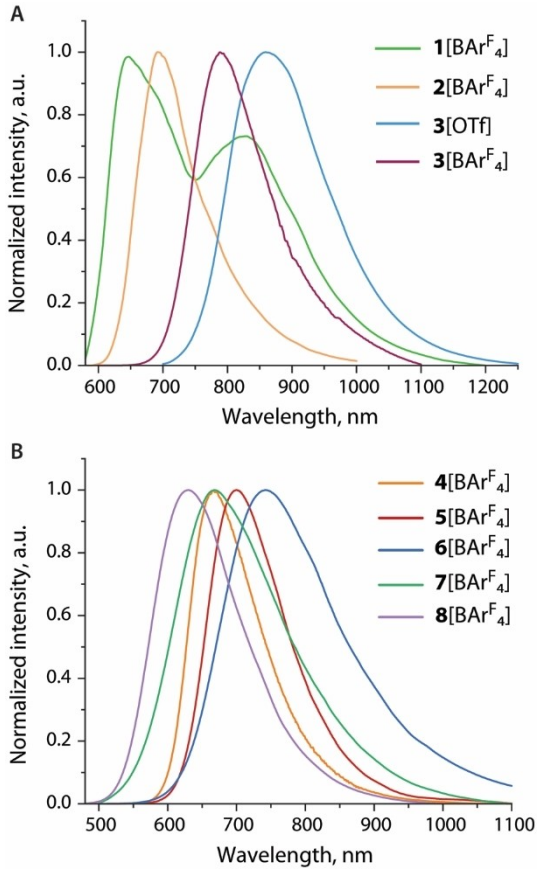

Figure 7. Normalized emission spectra of **1**–**3**[BAr^F_4], **3**[OTf] (A) and **4**–**8**[BAr^F_4] (B) in the solid state (solid) at room temperature.

740 nm/0.04). The congener compounds **5**[BAr^F_4] and **7**[BAr^F_4] with an ethynyl-phenylene or a thienyl-phenylene linkers attached to the anthracene core exhibit the lowest emission quantum yields not exceeding 0.01. The emission of diacene **8**[BAr^F_4] is represented by the single band at $\lambda_{em}=630$ nm, which is considerably blue-shifted compared to that found in CH_2Cl_2 solution ($\lambda_{em}=790$ nm).

Conclusions

In summary, we present a systematic study of anthracene-based donor-acceptor phosphonium dyes. The investigated series comprise compounds **1**–**3**[X] (X = triflate or $^-BAr^F_4$) with phosphacyclic acceptor motif including the novel phospha-spiro derivatives **3a**[OTf] and **3**[X], and salts **4**–**8**[BAr^F_4] bearing terminal $-^+PPh_2Me$ group. Cations **3a**$^+$ and **3**$^+$ represent a rare type of asymmetric phospha-spiro species, which comprise two different P-heterocycles; **3a**[OTf] is the first example of such compounds analyzed crystallographically. The experimental data, supported by theoretical analysis, reveal that bicyclic systems with a quaternized P atom are the most electron-accepting moieties in comparison to 6-membered P-heterocycles or acyclic cationic fragments. This results in the longest absorption wavelength ($\lambda_{abs}=575$ nm in CH_2Cl_2) and the smallest predicted energy gap for dye **3**[OTf]. Noteworthy, the emission of **3**[OTf] reaches 797 nm in solution (CH_2Cl_2) with the quantum yield of 0.12, whereas in amorphous solid it is further bathochromically shifted to 860 nm.

For **4**–**8**[BAr^F_4], bearing the same acyclic phosphonium substituent, variation of the electron-donating fragments was carried out. Low quantum efficiencies of **4**–**8**[BAr^F_4] and hypsochromic shift of solid-state fluorescence clearly make the phosphacyclic and particularly the phospha-spiro motifs the most appealing electron-accepting building blocks for the design of charge transfer D–A dyes, which could be of interest for imaging, optoelectronic and photovoltaic applications.

Experimental section

General considerations

Compounds *N,N*-diphenyl-4-(thien-2-yl)aniline,[38] 9-(2-bromophenyl)anthracene,[21] 9-(2-bromo-phenyl)-10-bromo-anthracene,[21] 4-[(9-(2-bromophenyl)anthracen-10-yl)ethynyl]-*N,N*-dimethylaniline,[21] 9-iodoanthracene,[39] 10-bromo-9-carbaldehyde anthracene,[40] 9,9′-bianthracene,[41] 10,10′-dibromo-9,9′-bianthracene,[42] 4-(*N,N*-diphenylamino)-benzeneboronic acid,[43] (4-(diphenylamino)phenyl)methanol,[44] diethyl (4-(diphenylamino)benzyl)phosphonate,[45] 4-ethynyl-*N,N*-diphenylaniline,[46] 10-bromo-9-(*N,N*-diphenylamino)-anthracene,[47] 5-chloro-dibenzo[b,d]phosphole,[24] phosphonium salts **1**[OTf], **2**[OTf], **4**[I][21,26] were prepared according to published procedures. The syntheses of other precursors and of the acyclic salts **4**–**8**[BAr^F_4], the details of physical measurements are described in the Supporting Information.

Synthetic procedures

3a[OTf]. The synthesis was carried out under a nitrogen atmosphere. A solution of $Cu(OTf)_2$ (0.35 g, 0.96 mmol) in acetonitrile (5 mL) was added to a solution of 5-(2-(anthracen-9-yl)phenyl)-5*H*-benzo[*b*]phosphindole (**p1**) (0.20 g, 0.46 mmol) in dichloromethane (15 mL) and the mixture was stirred for 10 min. The solvents were evaporated, and the residue was purified by column chromatography (Silica gel 70–230 mesh, 18×2.5 cm, eluent dichloromethane-methanol, 99:1→95:5 v/v mixture) to afford an orange product (240 mg, 90%). ESI-MS (m/z): $[M]^+$ 435.1310 (calcd 435.1303). ^1H NMR (CD_2Cl_2, 298 K; δ): 8.88 (d, J_{HH} 2.5 Hz, 1H, anthracene), 8.82 (dd, J_{HH} 9.0 Hz, 1.0 Hz, 1H, -anthracene), 8.58–8.60 (m, 1H, anthracene), 8.42 (dd, J_{HH} 8.0 Hz, 6.0 Hz, 1H, anthracene), 8.31 (d, J_{HH} 7.5 Hz, 1H, anthracene), 8.21 (br m, 2H, -C_6H_4-), 7.85–8.03 (m, 3H, -C_6H_4-+ phosphole), 7.76–7.83 (m, 4H, anthracene+-C_6H_4-+phosphole), 7.37–7.71 (m, 6H, -C_6H_4-+-phosphole). $^{31}P\{^1H\}$ NMR (CD_2Cl_2, 298 K; δ): 6.2 (s) ppm. $^{13}C\{^1H\}$ NMR (126 MHz, CD_2Cl_2, 298 K; δ): 140.8 (d, $J_{CP}=8$ Hz), 138.1 (d, $J_{CP}=3$ Hz), 137.2, 135.5 (d, $J_{CP}=11$ Hz), 135.2 (d, $J_{CP}=3$ Hz), 134.2, 134.1, 132.6, 132.2, 131.6, 131.4, 130.2 (d, $J_{CP}=9$ Hz), 129.7, 129.4, 129.3, 127.5, 126.6, 126.5, 126.4, 126.2, 125.4 (d, $J_{CP}=18$ Hz), 124.1 (d, $J_{CP}=9$ Hz), 112.6, 107.8. $^{19}F\{^1H\}$ NMR (CD_2Cl_2, 298 K; δ): –78.9 (s). Anal. Calc. for $C_{33}H_{20}F_3O_3PS$: C, 67.81; H, 3.45; S, 5.48; Found: C, 67.28; H, 3.67; S, 5.56.

3[OTf]. The synthesis was carried out under a nitrogen atmosphere. A solution of $Cu(OTf)_2$ (110 mg, 0.31 mmol) and trifluoromethanesulfonic acid (0.03 mL, 0.30 mmol) in acetonitrile (5 mL) was added to a solution of 4-[(10-(2-(5*H*-benzo[*b*]phosphindol-5-yl)phenyl)anthracen-9-yl)ethynyl]-*N,N*-dimethylaniline (**p2**) (84 mg,

0.15 mmol) in dichloromethane (10 mL). The mixture was stirred for 10 min., then an excess diethylamine (2 mL) was added and the solvents were evaporated. The resulting dark residue was purified by column chromatography (Silica gel 70–230 mesh, 18×2.5 cm, eluent dichloromethane-methanol, 99:1→95:5 v/v mixture) to afford dark violet product (70 mg, 66%). ESI-MS (m/z): $[M]^+$ 578.2022 (calcd 578.2037). ^{1}H NMR (CD_2Cl_2, 298 K; δ): 9.17 (d, J_{HH} 8.0 Hz, 1H, anthracene), 8.87 (d, J_{HH} 8.0 Hz, 1H, -C_6H_4-), 8.71 (d, J_{HH} = 8.5 Hz, 1H, phosphole), 8.28 (dd, J_{HH} = 8.0 Hz, 6.0 Hz, 1H, anthracene), 7.67–8.30 (m, 17H, -C_6H_4- + anthracene + phosphole + -C_6H_4-NMe_2), 6.77 (d, J_{HH} 8.5 Hz, 2H, -C_6H_4-NMe_2), 3.05 (s, 6H, -NMe_2). ^{31}P{^{1}H} NMR (CD_2Cl_2, 298 K; δ): 6.7 (s) ppm. ^{13}C (CD_2Cl_2, 298 K; δ) 151.2, 140.8, 136.8, 136.7, 135.3 (d, J_{CP} = 9 Hz), 135.0, 134.4, 134.1 (d, J_{CP} = 10 Hz), 133.9, 133.3, 132.0 (d, J_{CP} = 10 Hz), 131.2, 129.2, 129.1, 128.1, 127.9, 126.8, 125.8 (d, J_{CP} = 16 Hz), 125.3, 123.9, 111.8, 109.0, 108.1, 84.5. ^{19}F{^{1}H} NMR (CD_2Cl_2, 298 K; δ): −78.9 (s) ppm. ^{19}F{^{1}H} NMR (CD_2Cl_2, 298 K; δ): −78.9 (s) ppm. Anal. Calc. for $C_{43}H_{29}F_3NO_3PS$: C, 70.97; H, 4.02; N, 1.92; S, 4.41; Found: C, 69.9; H, 4.19; N, 1.86; S, 3.95.

General procedure for anion metathesis. Sodium tetrakis[3,5-bis(trifluoromethyl)phenyl]borate (1.05 equiv.) was added to a solution of a triflate or iodide salt (1.00 equiv.) in diethylether/dichloromethane (5:1 v/v mixture, 5 mL). The suspension was stirred at room temperature for 20 min., then was filtered through a pad of Celite and evaporated. The crude product was extracted with diethyl ether (10 mL), and purified by column chromatography (aluminium oxide neutral 150 mesh, eluent dichloromethane-hexane, 2:1 v/v).

1[BAr^F_4]. Prepared from **1**[OTf]. Deep red amorphous solid (45%). ESI-MS (*m/z*): $[M]^+$ 680.2513 (calcd 680.2507). ^{1}H NMR (CD_2Cl_2, 298 K; δ): 8.68 (d, J_{HH} 8.8 Hz, 1H, anthracene), 8.49 (m, 1H, anthracene), 8.38 (dd, J_{HH} 8.0 and 5.8 Hz, 1H, anthracene), 8.05 (d, J_{HH} 8.8 Hz, 1H, anthracene), 7.91–7.99 (m, 3H, anthracene), 7.49–7.85 (m, 24H, $[Bar^F_4]^-$ + -P^+Ph_2, -C_6H_4-), 7.30–7.42 (m, 14H, -C_6H_4- + -NPh_2), 7.16 (tt, J_{HH} 7.4 and 1.1 Hz, 2H, -NPh_2). ^{13}C NMR (CD_2Cl_2, 298 K; δ): 162.6 (q), 149.0, 148.0, 144.1, 140.5, 135.0, 135.4, 134.6 (d, J_{CP} = 8 Hz), 134.3, 134.1, 133.6, 131.6, 129.3 (qq), 127.7, 127.0, 126.5, 125.0 (d, J_{CP} = 15 Hz), 124.3, 123.8, 121.1, 118.1 (sept). ^{31}P{^{1}H} NMR (CD_2Cl_2, 298 K; δ): 5.7 (s, 1P, P^+_{cycl}). ^{31}P{^{1}H} NMR (CD_2Cl_2, 298 K; δ): 5.7 (s, 1P, P^+_{cycl}). Anal. Calcd. for $C_{82}H_{47}P_1N_1F_{24}B_1$: C, 63.79; H, 3.07; N, 0.91. Found C, 63.90; H, 2.77; N, 1.01.

2[BAr^F_4]. Prepared from **2**[OTf]. Purple solid (66%). Single crystals for the XRD structural analysis were obtained by slow diffusion of heptane into a dichloromethane solution of **2**[BAr^F_4] at room temperature. ESI-MS (*m/z*): $[M]^+$ 580.2168 (calcd 580.2194). ^{1}H NMR (CD_2Cl_2, 298 K; δ): 9.31 (dt, J_{HH} 8.3 and 1.4 Hz, 1H, anthracene), 8.81 (d, J_{HH} 8.6 Hz, 1H, anthracene), 8.54 (d, J_{HH} 8.6 Hz, 1H, anthracene), 8.24 (dd, J_{HH} 8.1 and 5.6 Hz, 1H, anthracene), 7.32–8.08 (m, 31H, anthracene + -P^+Ph_2, $[Bar^F_4]^-$ + -C_6H_4-), 6.74 (d, J_{HH} 9 Hz, 2H, -C_6H_4-), 3.10 (s, 6H, Me). ^{13}C{^{1}H} NMR (CD_2Cl_2, 298 K; δ): 163.1, 162.6, 162.1, 162.6 (q), 151.8, 140.4 (d, J_{CP} = 5 Hz), 137. 4 (d, J_{CP} = 8 Hz), 136.6, 136.4, 135.4, 135.0, 135.3, 134.5, 134.4, 134.3, 134.2, 133.9, 131.5, 131.3, 131.1, 131.0, 130.7, 130.6, 129.6 (qq), 128.6 (d, J_{CP} = 12 Hz), 127.4, 126.5, 126.2, 125.8 (q), 123.8, 121.1, 118.1(sept), 115.1, 114.2, 112.4, 111.6, 110.6, 109.5, 108.6, 85.0, 54.6, 54.0, 53.5, 40.5. ^{31}P{^{1}H} NMR (CD_2Cl_2, 298 K; δ): 5.7 (s, 1P, P^+_{cycl}). Anal. Calcd. for $C_{74}H_{43}P_1N_1F_{24}B_1$: C, 61.56; H, 3.00; N, 0.97. Found C, 61.80; H, 2.86; N, 1.01.

3[BAr^F_4]. Prepared from **3**[OTf]. Purple solid (84%). ^{1}H NMR (CD_2Cl_2, 298 K; δ): 9.25 (d, J_{HH} 9.8 Hz, 1H, -anthracene-), 8.94 (d, J_{HH} 7.3 Hz, 1H, –C_6H_4–), 8.77 (d, J_{HH} = 8.4 Hz, 1H, -phosphole-), 8.36 (dd, J_{HH} = 7.9 Hz, 6.2 Hz, 1H, -anthracene-), 7.51–8.25 (m, 29H, $[BAr^F_4]^-$ + -C_6H_4– + anthracene + phosphole + -C_6H_4-NMe_2), 6.78 (d, J_{HH} 9.0 Hz, 2H, -C_6H_4-NMe_2), 3.06 (s, 6H, -NMe_2). ^{13}C (CD_2Cl_2, 298 K; δ) 161.8 (m), 151.3, 137.0, 135.2, 135.07, 135.0, 134.8, 134.2 (d, J = 10 Hz), 134.2, 133.9, 133.3, 131.9, 131.8 (d, J_{CP} = 13 Hz), 131.3, 130.4 (d, J_{CP} = 10 Hz), 129.2, 129.0, 128.8, 128.5, 128.2, 128.0, 127.9, 126.8, 126.6, 126.5, 125.7, 125.5 (d, J_{CP} = 12 Hz), 125.1, 125.0, 123.8, 123.5, 121.4, 117.5, 112.5, 111.8, 109.2, 108.1, 108.0, 107.4, 84.5, 39.9. ^{31}P{^{1}H} NMR (CD_2Cl_2, 298 K; δ): 6.72 (s, 1P, P^+_{cycl}) ppm. ^{19}F{^{1}H} NMR (CD_2Cl_2, 298 K; δ): −63.0 (s) ppm. Anal. Calc. for $C_{74}H_{41}BF_{24}NP$: C, 61.64; H, 2.87; N, 0.97; Found: C, 61.10; H, 2.97; N, 0.88.

Supporting Information

The authors have cited additional references within the Supporting Information.[48]

Deposition Number(s) 2253592 (for **2**[BAr^F_4]), 2253593 (for **3a**[OTf]) contain(s) the supplementary crystallographic data for this paper. These data are provided free of charge by the joint Cambridge Crystallographic Data Centre and Fachinformationszentrum Karlsruhe Access Structures service.

Acknowledgements

Financial support from the Academy of Finland (decisions 317903 and 351618, I.O.K.; decision 339544, J.J.S.; Flagship Programme, Photonics Research and Innovation PREIN, decision 320166), Alexander von Humboldt and Otto A. Malm Foundations (A.B.), the Spanish Ministry of Science and Innovation (C.R.-N., projects MCIN/AEI/10.13039/501100011033/ and SBPLY/21/180501/000185) and the National Science and Technology Council (NSTC), Taiwan, are gratefully acknowledged.

Conflict of Interests

The authors declare no conflict of interest.

Data Availability Statement

The data are available from Cambridge Crystallographic Data Centre (https://www.ccdc.cam.ac.uk/structures/), in the Supporting Information, and from the authors on request.

Keywords: donor-acceptor systems · fluorescence · phosphonium salt · phosphorus heterocycles · spiro compounds

[1] a) M. Stępień, E. Gońka, M. Żyła, N. Sprutta, *Chem. Rev.* **2017**, *117*, 3479–3716; b) M. Hirai, N. Tanaka, M. Sakai, S. Yamaguchi, *Chem. Rev.* **2019**, *119*, 8291–8331; c) U. H. F. Bunz, J. Freudenberg, *Acc. Chem. Res.* **2019**, *52*, 1575–1587; d) X.-Y. Wang, X. Yao, A. Narita, K. Müllen, *Acc. Chem. Res.* **2019**, *52*, 2491–2505; e) G. J. Richards, J. P. Hill, *Acc. Chem. Res.* **2021**, *54*, 3228–3240.

[2] a) X. Feng, J.-Y. Hu, C. Redshaw, T. Yamato, *Chem. Eur. J.* **2016**, *22*, 11898–11916; b) M. Al Kobaisi, S. V. Bhosale, K. Latham, A. M. Raynor, S. V. Bhosale, *Chem. Rev.* **2016**, *116*, 11685–11796; c) N. Liang, D. Meng, Z. Wang, *Acc. Chem. Res.* **2021**, *54*, 961–975; d) V. M. Hertz, J. G. Massoth, M. Bolte, H.-W. Lerner, M. Wagner, *Chem. Eur. J.* **2016**, *22*, 13181–13188;

e) J. M. Farrell, C. Mützel, D. Bialas, M. Rudolf, K. Menekse, A.-M. Krause, M. Stolte, F. Würthner, *J. Am. Chem. Soc.* **2019**, *141*, 9096–9104.
[3] a) T. Baumgartner, *Acc. Chem. Res.* **2014**, *47*, 1613–1622; b) M. A. Shameem, A. Orthaber, *Chem. Eur. J.* **2016**, *22*, 10718–10735; c) D. Joly, P.-A. Bouit, M. Hissler, *J. Mater. Chem. C* **2016**, *4*, 3686–3698; d) R. Szűcs, P.-A. Bouit, L. Nyulászi, M. Hissler, *ChemPhysChem* **2017**, *18*, 2618–2630; e) A. Belyaev, P.-T. Chou, I. O. Koshevoy, *Chem. Eur. J.* **2021**, *27*, 537–552.
[4] a) Z. Fei, N. Kocher, C. J. Mohrschladt, H. Ihmels, D. Stalke, *Angew. Chem. Int. Ed.* **2003**, *42*, 783–787; b) T. Schillmöller, P. N. Ruth, R. Herbst-Irmer, D. Stalke, *Chem. Commun.* **2020**, *56*, 7479–7482; c) T. Schillmöller, R. Herbst-Irmer, D. Stalke, *Adv. Opt. Mater.* **2021**, *9*, 2001814.
[5] a) H. Xu, G. Xie, C. Han, Z. Zhang, Z. Deng, Y. Zhao, P. Yan, S. Liu, *Org. Electron.* **2012**, *13*, 1516–1525; b) Y. Zhao, L. Duan, X. Zhang, D. Zhang, J. Qiao, G. Dong, L. Wang, Y. Qiu, *RSC Adv.* **2013**, *3*, 21453–21460; c) G. Mallesham, C. Swetha, S. Niveditha, M. E. Mohanty, N. J. Babu, A. Kumar, K. Bhanuprakash, V. J. Rao, *J. Mater. Chem. C* **2015**, *3*, 1208–1224.
[6] a) Q. Fang, J. Li, S. Li, R. Duan, S. Wang, Y. Yi, X. Guo, Y. Qian, W. Huang, G. Yang, *Chem. Commun.* **2017**, *53*, 5702–5705; b) K. Behm, J. B. Essner, C. L. Barnes, G. A. Baker, J. R. Walensky, *Dalton Trans.* **2017**, *46*, 10867–10875; c) J. N. Smith, J. M. Hook, N. T. Lucas, *J. Am. Chem. Soc.* **2018**, *140*, 1131–1141.
[7] a) Y. Matano, A. Saito, T. Fukushima, Y. Tokudome, F. Suzuki, D. Sakamaki, H. Kaji, A. Ito, K. Tanaka, H. Imahori, *Angew. Chem. Int. Ed.* **2011**, *50*, 8016–8020; b) P.-A. Bouit, A. Escande, R. Szűcs, D. Szieberth, C. Lescop, L. Nyulászi, M. Hissler, R. Réau, *J. Am. Chem. Soc.* **2012**, *134*, 6524–6527; c) F. L. Laughlin, N. Deligonul, A. L. Rheingold, J. A. Golen, B. J. Laughlin, R. C. Smith, J. D. Protasiewicz, *Organometallics* **2013**, *32*, 7116–7121; d) F. Riobé, R. Szűcs, P.-A. Bouit, D. Tondelier, B. Geffroy, F. Aparicio, J. Buendía, L. Sánchez, R. Réau, L. Nyulászi, M. Hissler, *Chem. Eur. J.* **2015**, *21*, 6547–6556; e) M. P. Duffy, W. Delaunay, P. A. Bouit, M. Hissler, *Chem. Soc. Rev.* **2016**, *45*, 5296–5310; f) K. Yavari, W. Delaunay, N. De Rycke, T. Reynaldo, P. Aillard, M. Srebro-Hooper, V. Y. Chang, G. Muller, D. Tondelier, B. Geffroy, A. Voituriez, A. Marinetti, M. Hissler, J. Crassous, *Chem. Eur. J.* **2019**, *25*, 5303–5310; g) Z. Ma, Y. Liu, Z. Wang, W. Jiang, *Chem. Commun.* **2022**, *58*, 12321–12324.
[8] a) N. A. Takaesu, E. Ohta, L. N. Zakharov, D. W. Johnson, M. M. Haley, *Organometallics* **2017**, *36*, 2491–2493; b) E. Regulska, S. Christ, J. Zimmermann, F. Rominger, G. Hernandez-Sosa, C. Romero-Nieto, *Dalton Trans.* **2019**, *48*, 12803–12807; c) P. Hindenberg, J. Zimmermann, G. Hernandez-Sosa, C. Romero-Nieto, *Dalton Trans.* **2019**, *48*, 7503–7508; d) W. Ye, X. Li, B. Ding, C. Wang, M. Shrestha, X. Ma, Y. Chen, H. Tian, *J. Org. Chem.* **2020**, *85*, 3879–3886.
[9] a) T. Delouche, R. Mokrai, T. Roisnel, D. Tondelier, B. Geffroy, L. Nyulászi, Z. Benkö, M. Hissler, P.-A. Bouit, *Chem. Eur. J.* **2020**, *26*, 1856–1863; b) T. Delouche, E. Caytan, C. Quinton, T. Roisnel, M. Cordier, V. Dorcet, M. Hissler, P.-A. Bouit, *Chem. Eur. J.* **2021**, *27*, 11391–11397; c) T. Delouche, T. Roisnel, V. Dorcet, M. Hissler, P.-A. Bouit, *Eur. J. Inorg. Chem.* **2021**, *2021*, 1082–1089; d) R. Mokrai, A. Mocanu, M. P. Duffy, T. Vives, E. Caytan, V. Dorcet, T. Roisnel, L. Nyulászi, Z. Benkö, P.-A. Bouit, M. Hissler, *Chem. Commun.* **2021**, *57*, 7256–7259.
[10] a) Y. Ren, T. Baumgartner, *Inorg. Chem.* **2012**, *51*, 2669–2678; b) M. Arribat, E. Rémond, S. Clément, A. V. D. Lee, F. Cavelier, *J. Am. Chem. Soc.* **2018**, *140*, 1028–1034; c) P. Hindenberg, M. Busch, A. Paul, M. Bernhardt, P. Gemessy, F. Rominger, C. Romero-Nieto, *Angew. Chem. Int. Ed.* **2018**, *57*, 15157–15161; d) T. Delouche, A. Vacher, E. Caytan, T. Roisnel, B. Le Guennic, D. Jacquemin, M. Hissler, P.-A. Bouit, *Chem. Eur. J.* **2020**, *26*, 8226–8229.
[11] a) Y. Dienes, M. Eggenstein, T. Kárpáti, T. C. Sutherland, L. Nyulászi, T. Baumgartner, *Chem. Eur. J.* **2008**, *14*, 9878–9889; b) Y. Koyanagi, S. Kawaguchi, K. Fujii, Y. Kimura, T. Sasamori, N. Tokitoh, Y. Matano, *Dalton Trans.* **2017**, *46*, 9517–9527; c) J. D. R. Ascherl, C. Neiß, A. Vogel, J. Graf, F. Rominger, T. Oeser, F. Hampel, A. Görling, M. Kivala, *Chem. Eur. J.* **2020**, *26*, 13157–13162.
[12] a) C. Wang, A. Fukazawa, M. Taki, Y. Sato, T. Higashiyama, S. Yamaguchi, *Angew. Chem. Int. Ed.* **2015**, *54*, 15213–15217; b) N. Yoshikai, M. Santra, B. Wu, *Organometallics* **2017**, *36*, 2637–2645; c) R. A. Adler, C. Wang, A. Fukazawa, S. Yamaguchi, *Inorg. Chem.* **2017**, *56*, 8718–8725.
[13] a) Y. Ren, W. H. Kan, M. A. Henderson, P. G. Bomben, C. P. Berlinguette, V. Thangadurai, T. Baumgartner, *J. Am. Chem. Soc.* **2011**, *133*, 17014–17026; b) S. Wang, C. Yan, J. Shang, W. Wang, C. Yuan, H.-L. Zhang, X. Shao, *Angew. Chem. Int. Ed.* **2019**, *58*, 3819–3823.
[14] a) Y. Ren, T. Baumgartner, *J. Am. Chem. Soc.* **2011**, *133*, 1328–1340; b) X. He, J.-B. Lin, W. H. Kan, P. Dong, S. Trudel, T. Baumgartner, *Adv. Funct. Mater.* **2014**, *24*, 897–906.
[15] N. M.-W. Wu, M. Ng, W. H. Lam, H.-L. Wong, V. W.-W. Yam, *J. Am. Chem. Soc.* **2017**, *139*, 15142–15150.
[16] a) A. Saito, T. Miyajima, M. Nakashima, T. Fukushima, H. Kaji, Y. Matano, H. Imahori, *Chem. Eur. J.* **2009**, *15*, 10000–10004; b) D. Wu, J. Zheng, C. Xu, D. Kang, W. Hong, Z. Duan, F. Mathey, *Dalton Trans.* **2019**, *48*, 6347–6352; c) T. Higashino, K. Ishida, T. Sakurai, S. Seki, T. Konishi, K. Kamada, K. Kamada, H. Imahori, *Chem. Eur. J.* **2019**, *25*, 6425–6438.
[17] S. Arndt, J. Borstelmann, R. Eshagh Saatlo, P. W. Antoni, F. Rominger, M. Rudolph, Q. An, Y. Vaynzof, A. S. K. Hashmi, *Chem. Eur. J.* **2018**, *24*, 7882–7889.
[18] C. Wang, M. Taki, Y. Sato, Y. Tamura, H. Yaginuma, Y. Okada, S. Yamaguchi, *PNAS* **2019**, *116*, 15817.
[19] F. Yao, M. Kong, B. Yan, Y. Li, Q. Guo, J. Li, S. Wang, X. Guo, R. Hu, Y. Qian, Q. Fan, G. Yang, *Adv. Mater. Technol.* **2020**, *5*, 1901035.
[20] a) M. Grzybowski, M. Taki, K. Senda, Y. Sato, T. Ariyoshi, Y. Okada, R. Kawakami, T. Imamura, S. Yamaguchi, *Angew. Chem. Int. Ed.* **2018**, *57*, 10137–10141; b) Y. Fang, G. N. Good, X. Zhou, C. I. Stains, *Chem. Commun.* **2019**, *55*, 5962–5965; c) Y. Sugihara, N. Inai, M. Taki, T. Baumgartner, R. Kawakami, T. Saitou, T. Imamura, T. Yanai, S. Yamaguchi, *Chem. Sci.* **2021**, *12*, 6333–6341; d) H. Zhang, L. Shi, K. Li, X. Liu, M. Won, Y.-Z. Liu, Y. Choe, X.-Y. Liu, Y.-H. Liu, S.-Y. Chen, K.-K. Yu, J. S. Kim, X.-Q. Yu, *Angew. Chem. Int. Ed.* **2022**, *61*, e202116439.
[21] A. Belyaev, Y.-T. Chen, Z.-Y. Liu, P. Hindenberg, C.-H. Wu, P.-T. Chou, C. Romero-Nieto, I. O. Koshevoy, *Chem. Eur. J.* **2019**, *25*, 6332–6341.
[22] A. de Cózar, C. Romero-Nieto, *Inorg. Chem.* **2023**, *62*, 4097–4105.
[23] D. Hellwinkel, *Chem. Ber.* **1966**, *99*, 3668–3671.
[24] H. T. Teunissen, C. B. Hansen, F. Bickelhaupt, *Phosphorus Sulfur Silicon Relat. Elem.* **1996**, *118*, 309–312.
[25] A. Belyaev, Y.-T. Chen, S.-H. Su, Y.-J. Tseng, A. J. Karttunen, S. P. Tunik, P.-T. Chou, I. O. Koshevoy, *Chem. Commun.* **2017**, *53*, 10954–10957.
[26] A. Belyaev, Y.-H. Cheng, Z.-Y. Liu, A. J. Karttunen, P.-T. Chou, I. O. Koshevoy, *Angew. Chem. Int. Ed.* **2019**, *58*, 13456–13465.
[27] a) G. P. Schiemenz, R. Bukowski, L. Eckholtz, B. Vamskühler, *Z. Naturforsch. B* **2000**, *55*, 12–20; b) S. Nieto, P. Metola, V. M. Lynch, E. V. Anslyn, *Organometallics* **2008**, *27*, 3608–3610.
[28] a) D. Hellwinkel, *Chem. Ber.* **1965**, *98*, 576–587; b) T. Agou, M. D. Hossain, T. Kawashima, K. Kamada, K. Ohta, *Chem. Commun.* **2009**, 6762–6764; c) K. Hazin, D. P. Gates, *Can. J. Chem.* **2018**, *96*, 526–533.
[29] H. Umezawa, S. Okada, H. Oikawa, H. Matsuda, H. Nakanishi, *Bull. Chem. Soc. Jpn.* **2005**, *78*, 344–348.
[30] P. Gautam, C. P. Yu, G. Zhang, V. E. Hillier, J. M. W. Chan, *J. Org. Chem.* **2017**, *82*, 11008–11020.
[31] C. Reichardt, *Chem. Rev.* **1994**, *94*, 2319–2358.
[32] T.-C. Lin, Z.-Y. Liu, S.-H. Liu, I. O. Koshevoy, P.-T. Chou, *JACS Au* **2021**, *1*, 282–293.
[33] X. Chai, X. Cui, B. Wang, F. Yang, Y. Cai, Q. Wu, T. Wang, *Chem. Eur. J.* **2015**, *21*, 16754–16758.
[34] a) Y. Koyanagi, Y. Kimura, Y. Matano, *Dalton Trans.* **2016**, *45*, 2190–2200; b) J. N. Gayton, S. Autry, R. C. Fortenberry, N. I. Hammer, J. H. Delcamp, *Molecules* **2018**, *23*, 3051.
[35] a) J. J. Piet, W. Schuddeboom, B. R. Wegewijs, F. C. Grozema, J. M. Warman, *J. Am. Chem. Soc.* **2001**, *123*, 5337–5347; b) P. Zhang, W. Dou, Z. Ju, L. Yang, X. Tang, W. Liu, Y. Wu, *Org. Electron.* **2013**, *14*, 915–925; c) S. Kang, H. Lee, Y. Shim, S. Park, J. Park, *Dyes Pigm.* **2020**, *181*, 108555.
[36] a) Y. Haketa, H. Maeda, *Chem. Commun.* **2017**, *53*, 2894–2909; b) G. Li, Y. Xu, Q. Kong, W. Zhuang, Y. Wang, *J. Mater. Chem. C* **2017**, *5*, 8527–8534.
[37] a) N. Adarsh, A. S. Klymchenko, *Nanoscale* **2019**, *11*, 13977–13987; b) A. H. Ashoka, A. S. Klymchenko, *ACS Appl. Mater. Interfaces* **2021**, *13*, 28889–28898.
[38] A. Leliège, P. Blanchard, T. Rousseau, J. Roncali, *Org. Lett.* **2011**, *13*, 3098–3101.
[39] M. Shao, P. Dongare, L. N. Dawe, D. W. Thompson, Y. Zhao, *Org. Lett.* **2010**, *12*, 3050–3053.
[40] Y. Zhang, Z. Jiao, W. Xu, Y. Fu, D. Zhu, J. Xu, Q. He, H. Cao, J. Cheng, *New J. Chem.* **2017**, *41*, 3790–3797.
[41] Y. Yu, Z. Wu, Z. Li, B. Jiao, L. Li, L. Ma, D. Wang, G. Zhou, X. Hou, *J. Mater. Chem. C* **2013**, *1*, 8117–8127.
[42] P. Natarajan, M. Schmittel, *J. Org. Chem.* **2013**, *78*, 10383–10394.
[43] X. Yang, Y. Zhao, X. Zhang, R. Li, J. Dang, Y. Li, G. Zhou, Z. Wu, D. Ma, W.-Y. Wong, X. Zhao, A. Ren, L. Wang, X. Hou, *J. Mater. Chem.* **2012**, *22*, 7136–7148.
[44] H. Tian, X. Yang, R. Chen, R. Zhang, A. Hagfeldt, L. Sun, *J. Phys. Chem. C* **2008**, *112*, 11023–11033.
[45] S. Zheng, S. Barlow, T. C. Parker, S. R. Marder, *Tetrahedron Lett.* **2003**, *44*, 7989–7992.

[46] L. Wang, L. Yin, L. Wang, B. Xie, C. Ji, Y. Li, *Dyes Pigm.* **2017**, *140*, 203–211.
[47] K. S. Kisel, T. Eskelinen, W. Zafar, A. I. Solomatina, P. Hirva, E. V. Grachova, S. P. Tunik, I. O. Koshevoy, *Inorg. Chem.* **2018**, *57*, 6349–6361.
[48] a) E. C.-H. Kwok, D. P.-K. Tsang, M.-Y. Chan, V. W.-W. Yam, *Chem. Eur. J.* **2013**, *19*, 2757–2767; b) S.-C. Yiu, P.-Y. Ho, Y.-Y. Kwok, X. He, Y. Wang, W.-H. Yu, C.-L. Ho, S. Huang, *Chem. Eur. J.* **2022**, *28*, e202104575; c) *APEX2 - Software Suite for Crystallographic Programs*, Bruker AXS, Inc., Madison, WI, USA, **2010**; d) *APEX3 - Software Suite for Crystallographic Programs*, Bruker AXS Inc., Madison, WI, USA, **2015**; e) G. M. Sheldrick, *Acta Crystallogr. C: Struct. Chem.* **2015**, *71*, 3–8; f) L. J. Farrugia, *J. Appl. Crystallogr.* **2012**, *45*, 849–854; g) O. V. Dolomanov, L. J. Bourhis, R. J. Gildea, J. A. K. Howard, H. Puschmann, *J. Appl. Crystallogr.* **2009**, *42*, 339–341; h) G. M. Sheldrick, *SADABS-2008/1 – Bruker AXS Area Detector Scaling and Absorption Correction*, Bruker AXS, Madison, Wisconsin, USA, **2008**; i) A. M. Brouwer, *Pure Appl. Chem.* **2011**, *83*, 2213–2228; j) M. J. Frisch, G. W. Trucks, H. B. Schlegel, G. E. Scuseria, M. A. Robb, J. R. Cheeseman, G. Scalmani, V. Barone, G. A. Petersson, H. Nakatsuji, X. Li, M. Caricato, A. V. Marenich, J. Bloino, B. G. Janesko, R. Gomperts, B. Mennucci, H. P. Hratchian, J. V. Ortiz, A. F. Izmaylov, J. L. Sonnenberg, Williams, F. Ding, F. Lipparini, F. Egidi, J. Goings, B. Peng, A. Petrone, T. Henderson, D. Ranasinghe, V. G. Zakrzewski, J. Gao, N. Rega, G. Zheng, W. Liang, M. Hada, M. Ehara, K. Toyota, R. Fukuda, J. Hasegawa, M. Ishida, T. Nakajima, Y. Honda, O. Kitao, H. Nakai, T. Vreven, K. Throssell, J. A. Montgomery Jr., J. E. Peralta, F. Ogliaro, M. J. Bearpark, J. J. Heyd, E. N. Brothers, K. N. Kudin, V. N. Staroverov, T. A. Keith, R. Kobayashi, J. Normand, K. Raghavachari, A. P. Rendell, J. C. Burant, S. S. Iyengar, J. Tomasi, M. Cossi, J. M. Millam, M. Klene, C. Adamo, R. Cammi, J. W. Ochterski, R. L. Martin, K. Morokuma, O. Farkas, J. B. Foresman, D. J. Fox, *Gaussian 16 Rev. C.01*, Wallingford, CT, **2016**.

Manuscript received: April 4, 2023
Accepted manuscript online: May 22, 2023
Version of record online: May 22, 2023